

Correlation dynamics between electrons and ions in the fragmentation of D_2 molecules by short laser pulses

X. M. Tong,* Z. X. Zhao and C. D. Lin
*J. R. Macdonald Laboratory, Physics Department,
 Kansas State University, Manhattan, KS 66506-2601*

We studied the recollision dynamics between the electrons and D_2^+ ions following the tunneling ionization of D_2 molecules in an intense short pulse laser field. The returning electron collisionally excites the D_2^+ ion to excited electronic states from there D_2^+ can dissociate or be further ionized by the laser field, resulting in $D^+ + D$ or $D^+ + D^+$, respectively. We modeled the fragmentation dynamics and calculated the resulting kinetic energy spectrum of D^+ to compare with recent experiments. Since the recollision time is locked to the tunneling ionization time which occurs only within fraction of an optical cycle, the peaks in the D^+ kinetic energy spectra provides a measure of the time when the recollision occurs. This collision dynamics forms the basis of the molecular clock where the clock can be read with attosecond precision, as first proposed by Corkum and coworkers. By analyzing each of the elementary processes leading to the fragmentation quantitatively, we identified how the molecular clock is to be read from the measured kinetic energy spectra of D^+ and what laser parameters be used in order to measure the clock more accurately.

I. INTRODUCTION

The fragmentation and ionization of D_2 by intense optical laser fields has been an active area of theoretical and experimental studies during the past decades [1, 2, 3, 4, 5]. In most of these experiments it was assumed that the D_2 molecule is ionized in the early phase of the laser field producing D_2^+ ion which is subsequently ionized by the laser. Mechanisms for the ionization of D_2^+ ion include bond softening (SO) [6], charge resonance enhanced ionization (CREI) [7, 8, 9, 10, 11, 12, 13], in addition to direct ionization by the laser field. The dissociation and ionization of D_2^+ in the laser field result in $D^+ + D$ or $D^+ + D^+$, with characteristic kinetic energies reflecting the internuclear separation of the breakup of D_2^+ at the time when it is excited or ionized. Thus bond softening and CREI, which produce distinct peaks in the D^+ ion kinetic energy spectra have been observed experimentally and predicted theoretically. These peaks can be understood without reference to the ionization of D_2 itself initially, i.e., the ionization of D_2 and D_2^+ can be treated as two independent events. However, recent experiments [2, 3, 4, 5] pointed out a new group of peaks in the D^+ ion spectra at the higher energy (about 5 eV to 10 eV per ion) which has now been attributed to the rescattering process [14, 15, 16, 17, 18, 19, 20, 21, 22, 23, 24]. In the rescattering process, the electron which is released by tunneling ionization is driven back by the laser field to collide with the residual D_2^+ ion to ionize it or to excite it. If the D_2^+ ion is excited, it can dissociate directly or be further ionized by the laser. In both cases, the D^+ ion will have kinetic energy (the reflection principle)

characteristic of the internuclear separation where the ionization occurs. This paper is to examine all the elementary processes that lead to the emission of D^+ ions by the rescattering process following the initial tunneling ionization of the D_2 molecule. The calculation will be performed for D_2 molecules only, but clearly the same model can be applied to H_2 with minor modifications.

In Sec. II we first discuss all the elementary processes that lead to the dissociation or ionization of D_2 molecules in a laser field. Starting with the tunneling ionization of D_2 , we address the following issues: (1) Calculation of the ionization rates of D_2 from its equilibrium distance using the molecular tunneling ionization (MO-ADK) theory [25]; (2) The classical trajectory of the ionized electron in the laser field and the Coulomb field of the D_2^+ ion, with initial longitudinal and transverse velocity distributions following the description of the ADK theory [23]; (3) The free propagation and spreading of the nuclear wave packet after the tunneling ionization of D_2 from its equilibrium distance; (4) Semi-empirical formulae for electron impact excitation cross sections of D_2^+ from the σ_g ground state to the first few excited electronic states, in particular, the first σ_u and π_u states. These cross sections have to be evaluated at all values of internuclear separations and for different alignment angles of D_2^+ with respect to the laser polarization direction; (5) Evaluation of tunneling ionization rates of D_2^+ from the excited σ_u and π_u states at each internuclear separation; (6) Follow the time evolution of dissociation and ionization dynamics to extract the kinetic energy spectra of the fragmentation products. While rates or cross sections for each of these elementary processes have been formulated, in the full calculation we only consider D_2 initially aligned perpendicular to the direction of the laser polarization. In Sec. III, the resulting kinetic energy spectra of D^+ are compared to the experiment of Niikura *et al.* [4]

*Contact: xmtong@phys.ksu.edu

where D^+ ions were detected without knowing whether the other fragmentation product is a D or a D^+ . In contradiction to the conclusion of this work where the main peak in the D^+ kinetic energy spectrum was attributed to the dissociation of D_2^+ following excitation to the σ_u electronic state, we conclude from our calculation that the main peak is due to the further ionization of the excited D_2^+ by the laser. This has the consequence that the molecular clock we read is at a different time from the one read in Niikura *et al.* [4]. We further analyzed the contributions of the total kinetic energy spectra of D^+ resulting from the different excited electronic states, from dissociation or ionization, and from rescattering at the first return, the third return, or higher returns. The simulated D^+ kinetic energy spectra from ionization also were compared to the recent experiment of Alnaser *et al.* [26]. From our analysis, we conclude that the fragmentation of D_2 can be used as a molecular clock based on the rescattering dynamics. The clock can be read more accurately if the laser pulse is chosen at the lower intensity and with a shorter duration. With such a clock, the time duration can be read with an accuracy of fraction of a femtosecond without the attosecond laser pulses. Equivalently this means that the distance between the two nuclei can be read with an accuracy of fractions of an Angstrom. This can be achieved experimentally by comparing kinetic energy spectra for experiments carried out at different mean laser wavelengths, or by comparing the kinetic energy spectra of D^+ and H^+ from the fragmentation of D_2 and H_2 , respectively, in the same laser pulse. We finish this paper with a summary and conclusion in Sec. IV.

II. THE THEORETICAL MODEL

A. The elementary processes

The schematic of the physical processes leading to the fragmentation of D_2^+ ion following the ionization of D_2 molecule in an intense laser pulse is depicted in Fig. 1. The D_2 molecule is first ionized at t_0 near the peak of the laser pulse, releasing an electron into the oscillating laser field. At t_1 , the electron is driven back to the molecular ion, to excite the other electron in the ion to one of the higher excited electronic states, or to ionize it. We will be dealing with peak laser intensities such that the returning electron does not have enough energy to ionize D_2^+ . In the meanwhile, the nuclear wave packet propagates from its mean internuclear distance $R_0=1.4$ a.u. at t_0 to $R_1=1.6$ a.u. at t_1 . Thus the electron impact excitation probabilities of the molecular ion by the returning electron have to be calculated for D_2^+ with a vibrational distribution $\chi^2(R, t_1)$. This distribution is indicated in the second row of Fig. 1. Once the D_2^+ is in the excited state, represented by the curve labelled σ_u and π_u in Fig. 1, the D_2^+ can dissociate directly to $D^+ + D$, or it can be further ionized by the laser at t'_1 when the elec-

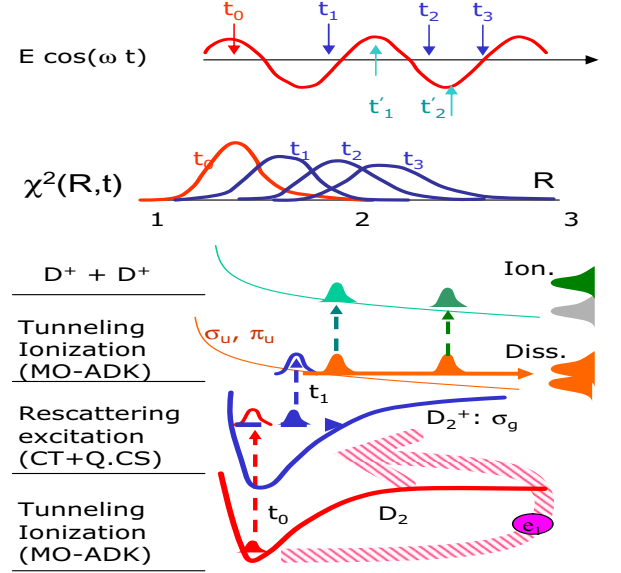


FIG. 1: Schematic of the major physical processes leading to the formation of D^+ ion by the dissociation or ionization of D_2^+ . The first row depicts the oscillating electric field of the laser. The second row shows the spreading of the vibrational wave packet after the initial tunneling ionization. At t_0 the D_2 molecule is ionized. The tunneled electron returns to rescatter with the D_2^+ ion at t_1 where it excites D_2^+ to the excited σ_u or π_u electronic states. The excited D_2^+ can dissociate along these repulsive potential curves, or further ionized by the laser to produce D^+ ions by Coulomb explosion, to produce characteristic kinetic energy spectra of the fragments. For more detailed description, see Text.

tric field of the laser returns to its peak value. If the D_2^+ is ionized at t'_1 , then it will fragment by Coulomb explosion to produce $D^+ + D^+$ ions. The total released kinetic energy for such a “two-step” process can be calculated.

The rescattering does not have to occur only at the first return time t_1 . Due to the attractive field from the molecular ion, the released electron can return to collide with the molecular ion at later times, i.e., after more than one optical cycle, following the initial ionization. For example, the return can occur at t_2 and t_3 , in the second optical cycle, or at t_4 and t_5 , in the third optical cycle, and so on. At these later times excitation and ionization occur at larger internuclear separations, thus the kinetic energies of the fragmented D^+ ion are smaller. In general the returning probabilities become small after three optical cycles. Following the general convention we call t_2 the second return and t_3 the third return, etc...

An important feature of the elementary processes described above is that the rescattering times t_i and the subsequent tunneling ionization time t'_i are relatively well locked to the clock t_0 of the initial ionization of D_2 . Since tunneling ionization occurs only near the peak of the

TABLE I: Relation between the returning time and the average nuclear separation for H_2^+ and D_2^+ .

return	time (fs)	< R > (a.u.)	
		H_2^+	D_2^+
t_1	1.9	1.8	1.6
t_3	4.3	2.5	2.1
t_5	7.0	3.0	2.6
t_7	9.6	3.2	3.0

laser field, t_0 spans only a fraction of an optical cycle. Similarly, t_i and t'_i are also restricted to within sub-fs accuracy. These precise clocks in turn define precise internuclear separations. For laser pulses with mean wavelength at 800 nm, the mean internuclear distances R_i for t_i ($i=1,3,5,7$) are shown in Table I for H_2 and D_2 . Note that at t_7 , the center of the vibrational wave packet for H_2^+ has already bounced back from the outer turning point, but not so for D_2^+ . A classical estimate shows that it takes 8.5 fs to reach its outer turning point. During these later times, the wave packet spreads significantly. The clock or the mean internuclear separation can be probed directly by the characteristic kinetic energy peaks of the fragmented D^+ ions. Changing the wavelength of the laser clearly will change the clocks and the mean internuclear separations. Replacing D_2 by H_2 will not change the clock but will change the mean internuclear distances.

To read the clock from the measured kinetic energy of the fragmented ion, however, there are a number of factors that make the clock “fuzzy”. First, the initial tunneling ionization occurs over an interval of about 0.3 fs near the peak of the laser field. The initial vibrational wave packet, taken to be the ground vibrational wavefunction of D_2 , according to the Frank-Condon principle, has a width of 0.2 nm. This vibrational wave packet will broaden as it expands to larger internuclear separation. The electron impact excitation probabilities and the MO-ADK rates also depend on internuclear separations. These factors would reduce the precision of the clock such that distinct peaks in the kinetic energy distribution of the fragmented ions are not as clearly separated. We model the rescattering process to check how accurately the molecular clock can be read from the kinetic energy spectra of the fragmented ions for different laser parameters.

We now describe the models used for calculating the rates and probabilities for each elementary process.

B. Tunneling ionization rates for molecules

We first discuss how the ionization rates of D_2 and D_2^+ in the laser fields are calculated. From the rescattering model above, we need the ionization rates for D_2 from the ground state, and for D_2^+ from the excited σ_u and π_u

states over the whole range of R . The rates are needed for different alignment of the molecules as well.

We calculated the tunneling ionization rates using the recently developed MO-ADK model [25]. It was obtained by extending the widely used ADK [27, 28] theory for atoms in a laser field to molecules. In the MO-ADK theory the ionization rates are given in semi-analytical expressions. For a diatomic molecule in a parallel static electric field, the ionization rate for a valence electron is given by

$$W_m(F) = \frac{B^2(m)}{2^{|m|}|m|!} \frac{1}{\kappa^{2Z_c/\kappa-1}} \times \left(\frac{2\kappa^3}{F}\right)^{2Z_c/\kappa-|m|-1} e^{-2\kappa^3/3F}, \quad (1)$$

with

$$B(m) = \sum_l C_{lm} (-1)^m \sqrt{\frac{(2l+1)(l+|m|)!}{2(l-|m|)!}}. \quad (2)$$

Atomic units are used unless otherwise indicated. In Eq. (1), κ is related to the ionization energy I_p by $\kappa = \sqrt{2I_p}$, l is the orbital angular momentum of the valence electron, m is its projection along the internuclear axis, Z_c is the effective charge seen by the valence electron in the asymptotic region and F is the field strength. In Eq. (2), the parameters C_{lm} are determined from the valence electron wave function of the molecule in the asymptotic region. The laser peak power will be given in units of $I_0 = 10^{14} \text{ W/cm}^2$ and the mean wavelength is 800 nm. If the molecule is aligned at an angle θ with respect to the laser polarization direction, the ionization rate is given by

$$W_m(F, \theta) = \sum_{m'} W_{m'}(F), \quad (3)$$

where $W_{m'}$ is given in Eq. (1) except that

$$B(m') = \sum_l C_{lm} D_{m',m}^l(0, \theta, 0) \times (-1)^{m'} \sqrt{\frac{(2l+1)(l+|m'|)!}{2(l-|m'|)!}}, \quad (4)$$

where the D -function expresses the rotation of the electronic wave function from the direction of the molecular axis to the laser polarization direction. In the MO-ADK model, Eq. (1) reduces to the traditional ADK model for atoms if l is taken to be the orbital angular momentum quantum number of the valence electron. For diatomic molecules, the summation over l is a consequence of expanding the two-center electronic wave function in terms of single-center atomic orbitals. The coefficients C_{lm} are functions of R and depend on the electronic states of the molecule.

For D_2 at the equilibrium internuclear separation, the parameters C_{lm} have been calculated by Tong *et al.* [25].

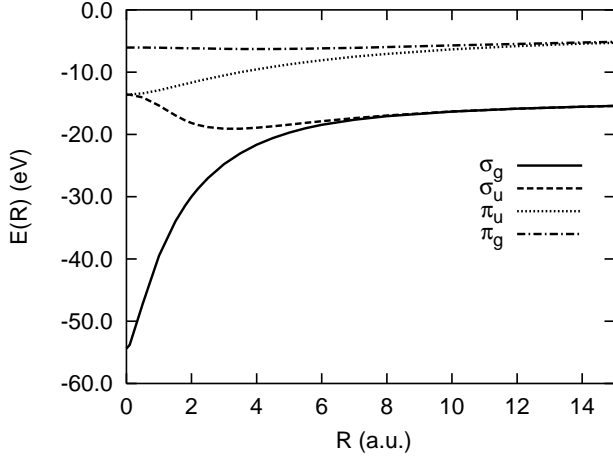


FIG. 2: Binding energies of D_2^+ as a function of internuclear separation.

Within the range of its ground vibrational wavefunction, it was found that the MO-ADK rates depend weakly on R . It was also found that the major component of $B(m=0)$ in Eq. (2) is $l=0$, for D_2 , thus the MO-ADK rates for D_2 depend weakly on the alignment of the molecule. The accuracy of the MO-ADK rates for D_2 at the equilibrium distance had been checked previously and found to be in good agreement with the result from *ab initio* calculations [29].

We next consider the ionization of D_2^+ in a laser field. Since the ionization rate depends sensitively on the ionization potential, in Fig. 2 we show the electronic binding energies $E_i(R)$ at each R of the first four electronic states of D_2^+ . The negative of the electronic binding energy is the ionization potential. The total potential energy of each electronic state is $U_i(R) = E_i(R) + 1/R$. For peak laser intensity in the range of 0.5 - $5 I_0$, estimate based on the simple ADK theory or the more complete MO-ADK theory shows that D_2^+ in the σ_g state will not be ionized by the laser except for R greater than about 5 a.u., while for π_u and π_g states the D_2^+ will be readily ionized because of the much smaller ionization potentials. Thus we need to calculate only the MO-ADK rates of D_2^+ in the σ_u state as a function of the internuclear distance R .

In Fig. 3 we show the calculated MO-ADK tunneling ionization rates at $F=0.06$ a.u. for the σ_u electronic state of D_2^+ , for R in the range of 1 - 6 a.u. and for alignment angle $\theta=0^\circ$ and 90° . At $\theta=0^\circ$, the MO-ADK rates have been checked against the “exact” static tunneling ionization rates calculated using the complex rotation method in the two-center system [30]. The MO-ADK rates tend to be somewhat higher, especially at small and large R region. For R greater than 6.0 the σ_u ionization energy is already very close to the ionization energy of atomic H, thus the ADK ionization rates of $H(1s)$ are used for $R > 6.0$. In the actual calculation, the coefficients C_{lm} are obtained for each R such that the MO-ADK rates can be readily calculated for any field strength, and any

alignment angle of the molecule using Eq. (3).

C. The rescattering model

Following the initial ionization of D_2 , a correlated electron wave packet and a vibrational wave packet are created at t_0 . The initial vibrational wave packet is taken to be the ground vibrational wavefunction of D_2 , assuming that the ionization process is fast and the Frank-Condon principle is valid. Due to the heavy mass of the nuclei, the vibrational motion is not modified by the subsequent laser field. The time evolution of the vibrational wave packet is thus described by

$$\chi(R, t) = \sum_v C_v \chi_v(R) e^{-i\varepsilon_v t}, \quad (5)$$

$$C_v = \int \chi_g(R) \chi_v(R) dR. \quad (6)$$

Here $\{\chi_v(R)\}$ and $\{\varepsilon_v\}$ are the vibrational wavefunction and vibrational energy of D_2^+ in the σ_g ground electronic state, respectively, and $\chi_g(R)$ is the the ground vibrational wave function of D_2 .

The rescattering model for describing the motion of the ionized electron in the subsequent laser field is modeled similar to the method used by Yudin and Ivanov [22, 23] for He. The ionized electron is treated classically, under the combined force from the laser field and the residual Coulomb interaction from the D_2^+ ion. For simplicity, the latter is approximated by an effective charge $Z_c=+1$ at the midpoint of the internuclear axis. To calculate the trajectory of the ionized electron, we solve the equation of motion (Newton’s second law), with the initial condition

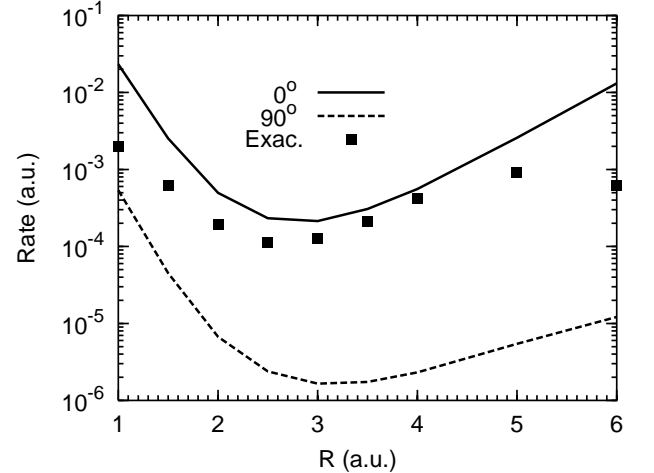


FIG. 3: Static MO-ADK ionization rates for D_2^+ molecules aligned parallel (solid curve) and perpendicular (dashed curve) to the electric field direction. The filled squares represent exact static ionization rates calculated using the complex rotation method [30] for parallel aligned molecules. The static field strength is 0.06 a.u..

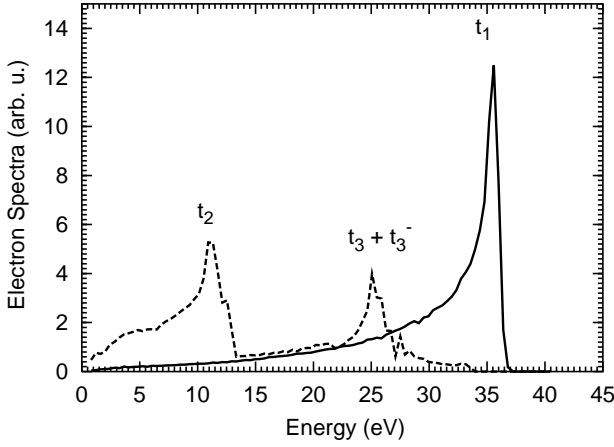


FIG. 4: Returning electron energy spectra for D_2 in a pulse laser with peak intensity of $1.5 I_0$ ($I_0=10^{14}$ W/cm 2) and pulse length of 40 fs obtained from the simulation.

that the ionized electron is at $(x,y,z)=(0,0,z_0)$ where z_0 is the tunneling position from the combined potential of the Coulomb field and the static electric field. The initial velocity \mathbf{v} is assumed to have a distribution from the ADK model,

$$g(\mathbf{v}) \propto e^{-\mathbf{v}^2 \kappa / F}. \quad (7)$$

In this model, the tunneled electron is ejected isotropically with a Gaussian distribution in velocity, i.e., we consider the ejected electron have initial velocity in both the transverse and the longitudinal directions. For each initial time t_0 or phase ϕ_0 that the ionized electron was born, the classical equation of motion was solved to obtain the trajectory. The distance of the electron from the center of D_2^+ ion is monitored for over seven optical cycles for longer pulses or till the end of the laser pulse if the pulse is shorter. The distance of closest approach of the electron from the ion and the time when this occurs for each trajectory are recorded. From these data, the impact parameter b and the collision energy T of the corresponding electron-ion impact (no laser field) excitation or ionization are obtained.

Figure 4 shows the probability distribution of finding the returning electron with kinetic energy T measured in the asymptotic region for a laser with peak intensity at $1.5 I_0$. If the residual Coulomb interaction from the D_2^+ ion is neglected, the expected maximum returning energy will be $3.17 U_P = 29$ eV, where U_P is the Pondermotive energy. The inclusion of Coulomb interaction increases this peak energy to about 35 eV.

In Fig. 4 we show three groups of returning electrons. In the first group, the electron was born at t_0 when the laser field has a positive phase ϕ_0 (i.e., beyond the peak field). It was driven outward and then back by the oscillating laser field to recollide with the D_2^+ ion within one optical cycle. This group is denoted by t_1 where the returning electron has peak current near 35 eV. The second group labelled t_2 denotes an electron which does

not collide with the ion at the first return, but at the second return about half a cycle later after the electron reverse its direction again. The kinetic energy for this group of electrons is smaller. The third group was denoted by $t_3 + t_3^-$. For the t_3 , the recollision occurs at the third return. For the t_3^- group, the electrons were born at a negative phase ϕ_0 [24], i.e., before the laser reaches the peak field. These negative phase electrons do not recollide with the ion in the first optical cycle when the field change direction since they were accelerated by an increasing field right after birth. Due to the Coulomb focusing by the ion they collide with the ion at the third return. Without the Coulomb focusing the negative phase birth would not contribute to the rescattering process. In calculating the returning electron energy distribution shown in Fig. 4 proper weights from the MO-ADK rates and the initial velocity distribution of the tunneling electron have been accounted for. In Fig. 4 we did not show the electron energy distributions from collisions occurred at returns after two optical cycles. The general trend is that at higher returns, the kinetic energy of the electron is smaller and the probability of rescattering is also smaller. In our calculations we have accounted for rescattering up to seven optical cycles for the long laser pulses.

D. Electron impact excitation and ionization probabilities

For each impact parameter b and kinetic energy T of the returning electron, we need to calculate the electron impact excitation and ionization cross sections of D_2^+ at each internuclear separation R . Different from the He^+ case, there are few experimental or theoretical data available for D_2^+ . Thus we have to generate the cross sections needed semi-empirically. For each total cross section $\sigma(T)$ at kinetic energy T , we assume that the probability for excitation or ionization at impact parameter b is given by

$$P_m(b, T) = \sigma(T) \frac{e^{-b^2/a_o^2}}{\pi a_o^2}, \quad (8)$$

$$a_o = \sqrt{2/\Delta E}, \quad (9)$$

where $T = v^2/2$ and ΔE is the excitation or ionization energy. Here, the b -dependence is taken to be the Gaussian form. For the rescattering in He, Yudin and Ivanov [22] have checked different forms of b -dependence and concluded that the results are rather insensitive to the precise functional form used.

For electron impact ionization cross section, we employ the empirical formula

$$\sigma_i(T, \Delta E) = \frac{\pi}{\Delta E^2} e^{1.5 * (\Delta E - 0.5) / T} f(T/\Delta E) \quad (10)$$

$$f(x) = (A \ln x + B(1 - \frac{1}{x}) - C \frac{\ln x}{x}) \frac{1}{x}. \quad (11)$$

where ΔE is the ionization energy. By fitting this formula to the accurate theoretical H(1s) ionization cross

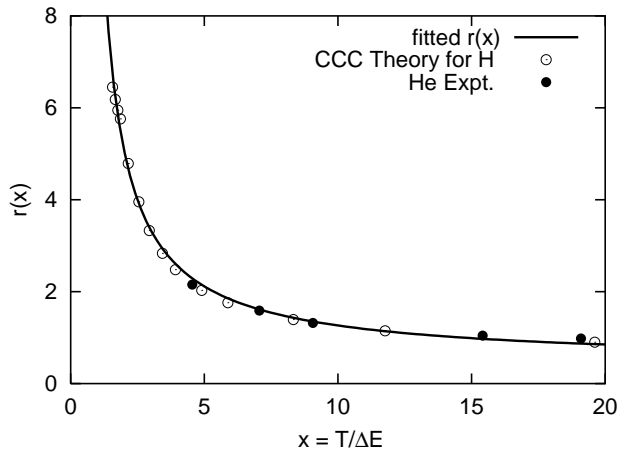


FIG. 5: Ratio of the electron impact excitation cross section to $2p_0$ with respect to $2p_1$ vs scaled excitation energy. Solid line is the fitted result from Eq. (12), open circles are from the calculation of Bray for H [33], and filled circles are from the He experimental measurement [34].

section [31] we obtained $A = 0.7213$, $B = -0.302$, $C = 0.225$. The fitted formula, when applied to He^+ , gives ionization cross sections in good agreement with the theoretical results of Bray [31] for He^+ as well. For D_2^+ at the equilibrium distance this formula also reproduces the recommended ionization cross section from NIST [32]. In this semi-empirical model, the molecular ion is treated as a point particle, thus the ionization cross section is independent of the alignment of the D_2^+ ion.

For the excitation process, it is clear from Fig. 2 that σ_u and π_u states will be the dominant channels populated via electron impact excitation from the ground σ_g state since they have the lowest excitation energies. There are no theoretical or experimental data available for such cross sections as functions of internuclear separations. Thus we will employ semi-empirical fitting procedure as well. We assume that the excitation cross section again can be fitted in the form of Eqs (10) and (11) as in ionization, except that ΔE now is the excitation energy and the number 0.5 in Eq (10) should be replaced by the excitation energy of the corresponding state in atomic hydrogen. From the tabulated $\text{H}(1s) \rightarrow \text{H}(2p)$ excitation cross section in Bray [31], we obtained $A = 0.7638$, $B = 1.1759$, $C = -0.6706$. The formula was further tested by comparing the predicted excitation cross section with the calculated one for $e^- + \text{He}^+(1s) \rightarrow e^- + \text{He}^+(2p)$. From the total $1s \rightarrow 2p$ excitation cross section, we can further distinguish excitation cross section to $2p_0$ or $2p_1$, with the direction of the incident electron beam as the quantization axis. The relative $2p_0$ and $2p_1$ cross sections can be calculated theoretically or experimentally from polarization or correlation measurements. (Note: $2p_{-1}$ cross section is identical to $2p_1$ cross section by symmetry.) In Fig. 5 we show the relative cross sections of $2p_0$ to $2p_1$ from the calculation of Bray [33] for H, plotted against scaled energy (with respect to the excitation energy). On

the same graph we display the same ratio for the excitation of He from $1s^2$ to $1s2p^1P^o$ from the experiment of Merabet *et al.* [34]. It appears that the both H and He data fall on the same curve when the collision energy is scaled with respect to the excitation energy. We fit the $2p_0$ to $2p_1$ cross section ratio by

$$r(x) = \frac{\sigma_0}{\sigma_1} = \frac{8.2\sqrt{1 + 1.1/x^2}}{x} + 0.44. \quad (12)$$

where $x = T/\Delta E$ is the scaled kinetic energy. Since the ratio for He does not differ much from the calculated ratio for H, this comparison convinces us to use the $r(x)$ in Eq. (12) to describe the ratio for D_2^+ as well. The $r(x)$ indicates that $m=0$ is the dominant magnetic component in the present interested energy regime.

To relate the $2p_0$ or $2p_1$ partial cross sections to the excitation cross sections of σ_u and π_u electronic states of D_2^+ , we need to know the alignment angle of the molecule. If the molecule is aligned along the laser field polarization direction (which is also the direction of the electron beam), the $2p_0$ cross section is the excitation to σ_u state and the $2p_1$ ($2p_{-1}$) cross section is for the excitation to the π_u state. If the molecule is aligned perpendicular to the laser polarization direction, then the role is reversed, i.e., $2p_1$ (or $2p_{-1}$) corresponds to the cross section of the σ_u excitation, and $2p_0$ cross section to the π_u excitation. For any arbitrary alignment angle θ of D_2^+ , we assume the total excitation cross sections to σ_u and π_u are given by

$$\sigma(\sigma_u) = \sigma_T(r_0 \cos^2 \theta + r_1 \sin^2 \theta) \quad (13)$$

$$\sigma(\pi_u) = \sigma_T(r_0 \sin^2 \theta + r_1 \cos^2 \theta). \quad (14)$$

$$\sigma_T = \sigma_0 + 2\sigma_1 \quad (15)$$

$$r_0 = \frac{\sigma_0}{\sigma_T} = \frac{r(x)}{r(x) + 2} \quad (16)$$

$$r_1 = \frac{2\sigma_1}{\sigma_T} = \frac{2}{r(x) + 2}. \quad (17)$$

The semi-empirically fitted electron impact ionization or excitation cross section formulae discussed so far are for a free electron colliding with an atomic or molecular ion. For the rescattering process, the two electrons in D_2 initially are in the singlet state ($S=0$). Thus in principle, one should just use singlet excitation or ionization cross sections, instead of the spin-averaged cross sections. We obtain the singlet cross sections from the total cross section following the empirical formula derived in Yudin and Ivanov [23] [their Eqs. (8) and (9)].

These empirical formulae allow us to calculate electron impact excitation cross sections from σ_g to σ_u and to π_u states at each internuclear separation and at each alignment of the D_2^+ ion. In Fig. 6 we compare the electron impact excitation cross sections at the equilibrium distance to σ_u and π_u states, for D_2^+ ions lying parallel and perpendicular to the incident electron direction which is also the direction of the laser polarization, respectively. When D_2^+ is aligned parallel to the laser polarization, impact excitation to σ_u is the dominant channel. The π_u

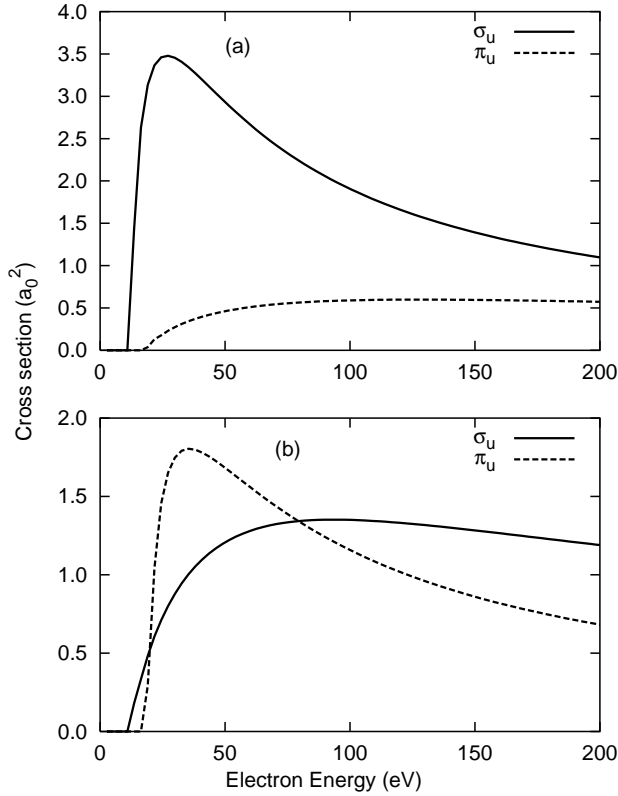


FIG. 6: Electron impact excitation cross sections to σ_u and π_u states of D_2^+ at the equilibrium distance. (a) The electron beam is parallel to the molecular axis; (b) the electron beam is perpendicular to the molecular axis.

cross sections are smaller due to two factors: (1) the π_u state has higher excitation energy, see Fig. 2; (2) the $2p_0$ state has larger cross sections than $2p_1$ for the electron energies considered, see Fig. 5. The situation is different when D_2^+ ion is aligned perpendicular to the laser polarization direction. Fig. 6(b) indicates that excitation to the π_u state is actually larger than that to the σ_u state, at least in the 20-80 eV energy region. Note that in the experiments of Niikura *et al.* [3, 4] the H_2^+ or D_2^+ were chosen to be perpendicular to the laser polarization direction. They assumed that electron impact excitation populates only the σ_u state, in disagreement with our analysis.

The semi-empirical formulae presented above allow us to calculate electron impact excitation cross sections to σ_u and π_u states averaged over the initially randomly distributed D_2^+ ions. We obtained the ratio of the cross section of σ_u with respect to π_u , and compared the result with the ratio obtained by Peek [35] where the impact excitation cross sections for different internuclear separations were calculated using the Born approximation. The agreement is quite good, with the average cross section for σ_u about a factor of two larger than for π_u . The absolute cross sections from Peek are larger since Born approximation was used.

We also consider the small contribution from excitation

to the $2s\sigma_g$ electronic state of D_2^+ . The empirical formula is chosen to be

$$\sigma_e(T, \Delta E) = \frac{1}{\Delta E^2} f(T/\Delta E) \quad (18)$$

$$f(x) = \frac{A}{1 + B/x} \frac{1}{x} \quad (19)$$

where the parameters $A = 0.17$, $B=1.53$ are obtained by fitting the formula to the $1s \rightarrow 2s$ excitation cross sections of H. This cross section is assumed to be independent of the alignment of the molecular ion.

E. Impact excitation probability

With all the elementary cross sections available, we can now calculate the probability distribution of exciting D_2^+ at a given internuclear separation R from the ground σ_g state to a specific excited electronic state or to ionization states by the returning electron where the returning electron originates from the ionization of D_2 molecule by the laser over a half optical cycle. The probability distribution is given by

$$\frac{dP_m}{dR} = \frac{\int \int P_m(b, T) \chi^2(R, t_r) g(\mathbf{v}) W(F \cos \phi) d\mathbf{v} d\phi}{\int \int g(\mathbf{v}) W(F \cos \phi) d\mathbf{v} d\phi}, \quad (20)$$

The subscript m stands for the excited states ($\sigma_u, \pi_u, \sigma_g$) or ionization. $P_m(b, T)$ is the impact excitation or ionization probability from Eq. (8). In this expression, W is the MO-ADK rate for ionizing D_2 at the static field $F \cos \phi$, where F is the peak field strength of the laser. For each ϕ , the tunneled electron leaves the molecule with an initial velocity \mathbf{v} , with a distribution governed by Eq. (7), i.e., effects due to both the longitudinal and transverse velocity distributions are included. For each initial velocity and initial position of the tunneled electron, the return time t_r at the distance of closest approach, the corresponding laser-free impact parameter b and kinetic energy T are calculated, and the excitation probability is also calculated. At each return time t_r , the distribution of the vibrational wave packet, $\chi^2(R, t_r)$, is used to calculate the probability of finding D_2^+ at internuclear separation R . In this expression the MO-ADK rates and the impact excitation probabilities to σ_u and π_u states depend on the alignment of molecules. The other quantities are isotropic. For D_2 initially aligned perpendicular to the direction of the linear polarization of the laser, the impact excitation probabilities at different R 's over half an optical cycle are shown in Fig. 7, where the peak laser intensity is $1.5 I_0$. Note that excitation probability to π_u is the largest, but to σ_u is also significant. On the other hand, excitation to $2s\sigma_g$ excited state and direct ionization by the rescattering electron are not important.

It is interesting to point out that the probability of excitation in Fig. 7 shows distinct sharp peaks as a function of R . To disentangle the source of these peaks, in Fig. 8 we examine the contributions to the π_u excitation probability according to whether the return time t_r falls within

one, two, three or four optical cycles after the tunneling electron is born. The excitation probabilities are larger for returns within one or two optical cycles. Within the first two optical cycles, the nuclear wave packets remain at small R with small spreading and the returning electron has more kinetic energy (see Fig. 4). For the higher returns the nuclear wave packet moves to larger R and spreads further and the smaller energies for the returning electron render the excitation probabilities smaller.

We comment once again that with the inclusion of Coulomb attraction on the motion of the rescattering electron, the maximum returning electron energy is not given by $3.17U_P=29$ eV for the present peak intensity, but rather by 35 eV, as seen from Fig. 4. This has the effect of enhancing the excitation to the π_u state as well.

For peak laser intensity of $1.5 I_0$ the results in Fig. 7 show that direct impact ionization of D_2^+ by the rescattering electron is very small. The rescattering mostly populates D_2^+ in the excited π_u and σ_u states. The dissociation of D_2^+ from an excited electronic state would release a total kinetic energy given by $U(R_0)-U(\infty)$, shared equally by D and D^+ , respectively. According to Fig. 7, excitation by the rescattering process peaks at characteristic internuclear separations related to characteristic rescattering time t_r , thus measurement of the D^+ fragment kinetic energies probes directly the recollision times. This forms the basis of molecular clocks in the experiments of Niikura *et al.* [3, 4]. However, as shown in Tong *et al.* [36] and in Alnaser *et al.* [26], the excited D_2^+ ions are still in the laser field and they can be further ionized by the lasers. Thus we need to calculate the kinetic energy spectra of D^+ resulting from Coulomb explosion after these excited D_2^+ ions are ionized by the laser.

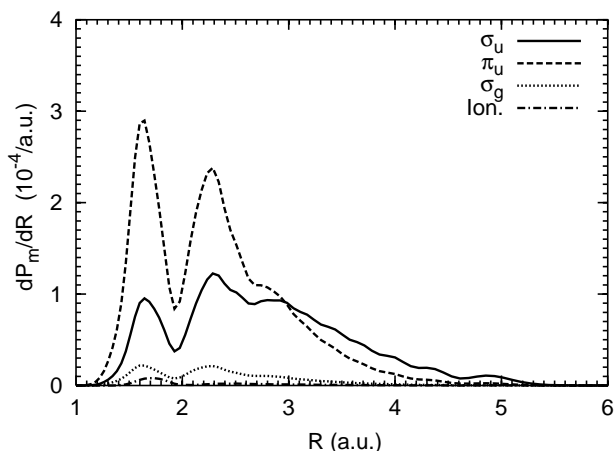


FIG. 7: Electron impact excitation and ionization probabilities of D_2^+ by the rescattering electron following tunneling ionization of D_2 by a short pulse laser with peak intensity of $1.5 I_0$ ($I_0=10^{14}$ W/cm²) and pulse length of 40 fs.

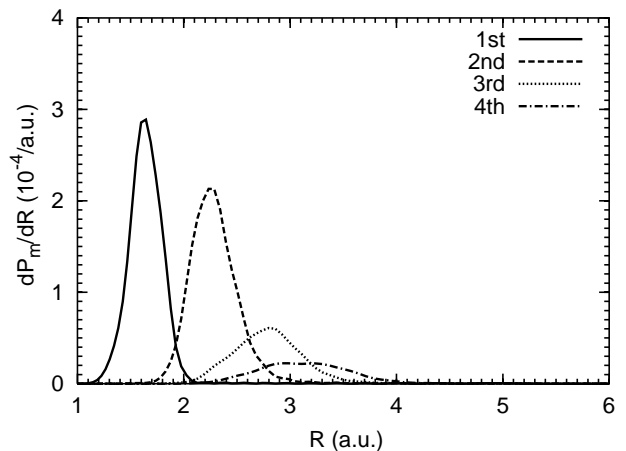


FIG. 8: Electron impact excitation probabilities by the rescattering electron to the π_u state in the first four optical cycles after D_2 molecules are ionized by a short pulse laser of peak intensity of $1.5 I_0$ ($I_0=10^{14}$ W/cm²) and pulse length of 40 fs.

F. Field ionization of excited D_2^+ ion

In this subsection we consider the ionization of D_2^+ from the excited electronic states. We emphasize that we will consider peak laser intensity within $0.5-5 I_0$ only where rescattering is important. In this intensity region, D_2^+ is readily ionized if it is in the π_u excited state since its saturation intensity is only about $0.1 I_0$ because of small ionization energy. Thus we need only to calculate the ionization rate of D_2^+ from the σ_u state. If the initial excitation to σ_u occurs at R , the total accumulated probability for ionizing an electron by the laser field from the σ_u state is

$$P_i(R, \infty) = 1 - e^{-\int W(R') dt} = 1 - e^{-\int_R^\infty W(R')/v(R') dR'}, \quad (21)$$

$$\text{with } \frac{1}{2}\mu v^2(R') = U(R) - U(R'). \quad (22)$$

where $W(R')$ is the MO-ADK tunneling ionization rate described in subsection A, μ is the reduced mass of the two nuclei, and $U(R)$ is the total potential energy of the σ_u state. The σ_u state created at R , followed by laser field ionization at R' will release a kinetic energy $E_i(R') = U(R) - U(R') + 1/R'$. Here we are more interested in the differential ionization probability which is given by

$$\frac{dP_i(R, R')}{dR'} = \frac{W(R')}{v(R')} e^{-\int_R^{R'} W(R'')/v(R'') dR''}, \quad (23)$$

or in terms of differential probability per unit of kinetic energy

$$\frac{dP_i(R, R')}{dE} = \frac{dP_i(R, R')}{dR'} \frac{dR'}{dU} \quad (24)$$

$$\frac{dR'}{dU} = \frac{1}{\left| \frac{dU(R')}{dR'} \right|} \quad (25)$$

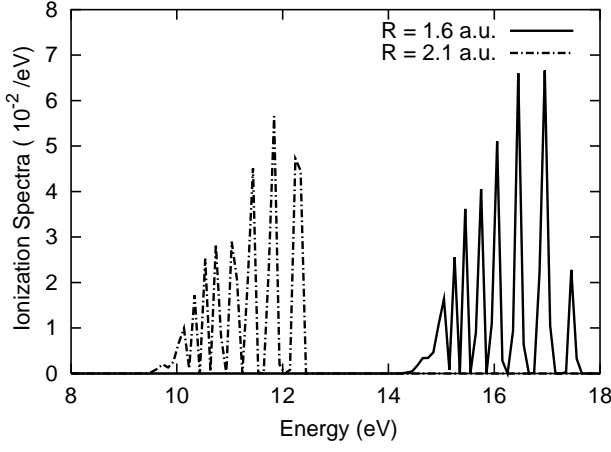


FIG. 9: Kinetic energy spectra of D^+ ion resulting from laser ionization of D_2^+ in the excited σ_u state, for ion reaching the excited state initially at $R=1.6$ a.u. (solid curve) and $R=2.1$ a.u. (dashed curve), respectively. Laser parameters: peak intensity 1.5×10^{14} W/cm², pulse length 40 fs.

Fig. 9 shows the expected ionization spectra from the σ_u state if it is initially created at two different R 's ($R=1.6$ and 2.1 a.u.), chosen to be the peak positions of the vibrational wave packet at the first and the third returns. Clearly, the early return releases more energy (higher energy peak). The spectra show many sharp peaks since ionization occurs only when the laser field is near its peak intensity at every half cycle.

To obtain the total ionization spectra, we need to add up contributions from initial ionization at all values of R , i.e.,

$$\frac{dP_{ion}}{dE} = \int \frac{dP_m}{dR} \frac{dP_i(R, R')}{dE} dR \quad (26)$$

This integration is important primarily only for ionization from the excited σ_u state. For other excited electronic states, due to the high ionization rate, ionization is complete within one cycle or less and we can set $R = R'$, and the differential ionization spectra for these excited electronic states are given by

$$\frac{dP_{ion}}{dE} = \frac{dP_m}{dR} \frac{dR}{dU}. \quad (27)$$

The total ionization spectra are obtained by adding up contributions from all the excited electronic states, and from the initial ionization by the rescattering electron (very negligible).

For the dissociation process, the energy spectra are obtained from

$$\frac{dP_{dis}}{dE} = (1 - P_i(R)) \frac{dP_m}{dR} \frac{dR}{dU}. \quad (28)$$

The total dissociation spectra are obtained by adding up contributions from all the excited electronic states. In reality, the dissociation comes from the σ_u excited state only. In all other excited electronic states the D_2^+ ions are immediately ionized by the laser in one optical cycle.

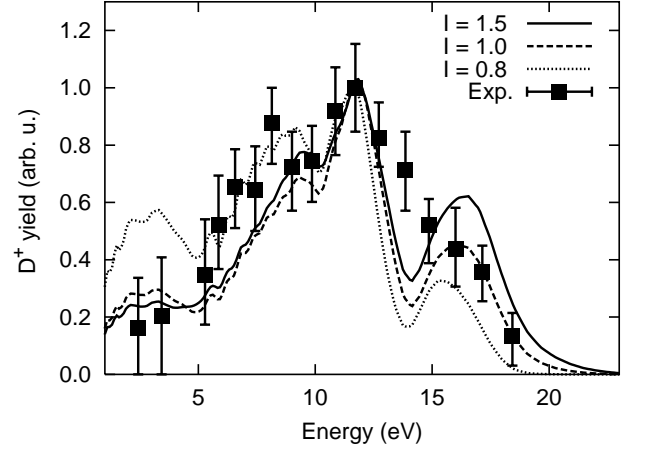


FIG. 10: D^+ yield at several laser intensities for a 35 fs pulse length. The experimental data are from Ref. [4] for $1.5 I_0$ where $I_0=10^{14}$ W/cm². The peak values from experiment and from theory for $1.5 I_0$ are normalized to each other. For peak intensities of $1.0 I_0$ and $0.8 I_0$, the yields have been multiplied by 1.4 and 3.0 respectively to have the same peak ion yield height.

III. RESULTS AND DISCUSSION

The kinetic energy spectra of D^+ ions can be determined without any coincidence, as in the experiments of Niikura *et al.* [3, 4], or by detecting the two D^+ ions in coincidence, as in the experiments of Staudte *et al.* [2] or in Alnaser *et al.* [26]. We will present our simulation results for both types of experiments.

A. Non-coincident D^+ kinetic energy spectra

In the experiments of Niikura *et al.* [3, 4], the kinetic energy of D^+ ion was measured in the direction perpendicular to the direction of laser polarization. The measured D^+ signals come from ionization and from dissociation. Thus,

$$Signal \propto 2 \frac{dP_{ion}}{dE} + \frac{dP_{dis}}{dE}. \quad (29)$$

In Fig. 10 the experimental D^+ kinetic energy spectra from Niikura *et al.* [4] are shown. The energy scale is the total breakup energy, or twice the energy of the D^+ ion. The experiment was performed for a pulse of 40 fs and peak intensity of $1.5 I_0$. We have shown simulations with the same laser parameters but with three peak laser intensities, at 1.5 , 1.0 and $0.8 I_0$. First we normalize the peak height at 12 eV between theory and experimental data at $1.5 I_0$. Since the peak positions do not vary with laser intensity, we can normalize the calculated spectra at the two other intensities as well, with a multiplicative factor of 1.4 and 3.0 for the 1.0 and $0.8 I_0$, respectively. If one compares the experimental spectra with the theoretical one calculated at the same $1.5 I_0$, clearly the

high energy peak near 16 eV from the theory is too high, while the theoretical spectra between 5 and 10 eV are somewhat too low. However it appears that the discrepancy can be reconciled if one takes into account of the volume effect in that the experimental spectra have to be integrated over a volume where the intensities are less than the peak value. The energy resolution and the finite acceptance angles can all contribute to the smoother experimental spectra. One of course should also take this “better agreement” with caution in view that the peak intensity of the laser is often not known precisely.

One of the major goals of the simulation is to unravel the origin of the structure in the kinetic energy spectra which in turn would provide insight of the working of the molecular clock. For this purpose, we show in Fig. 11 the calculated kinetic energy spectra, but separate the contributions from dissociation and ionization, and from rescattering occurred after one or two optical cycles, or equivalently, from the first (t_1) or the third returns(t_3), at two laser intensities, 1.5 and 0.8 I_0 . At the higher intensity, in this figure we notice: (1) ionization is much stronger than dissociation; (2) the peak from the third return (2nd cycle) is higher than from the first return;

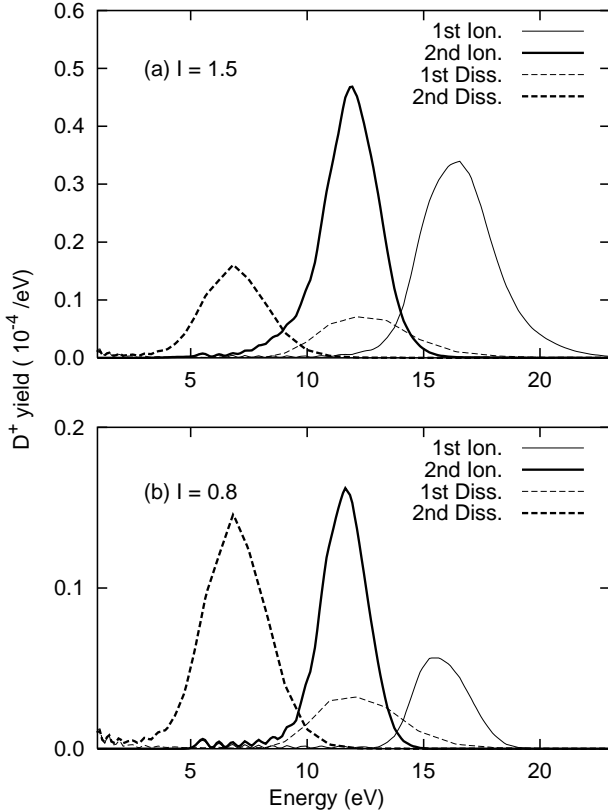


FIG. 11: Decomposition of D^+ ion yields into contributions from dissociation and ionization, and for rescattering occurring within the first and the second optical cycle after the initial tunneling ionization. The peak laser intensities are (a) $I = 1.5 I_0$ and (b) $I = 0.8 I_0$, where $I_0 = 10^{14} \text{ W/cm}^2$ and pulse length is 40 fs.

(3) The width of the peak from the first return is broader than the peak from the third return. The broadening is a consequence of the factor dR/dU in Eqs. (26) and (28) which is approximately given by R^2 . Another interesting observation is that the peak position of the dissociation spectra from the first return almost coincides with the peak position in the ionization spectra from the third return. This shift is due to the binding energy of the excited electronic states.

In Niikura *et al.*'s experiment [4] the peak at 12 eV was attributed to originate from the dissociation of D_2^+ via the σ_u curve at the first return. In other words, this peak reads the clock at t_1 . According to our simulation, the peak comes from ionization following rescattering at the third return, and this peak should read the clock at t_3 .

Contributions to the D^+ signal from dissociation do become more important at lower laser intensity, as shown in Fig. 11(b). Even at this intensity, the peak at 12 eV still comes mostly from the ionization following rescattering at t_3 instead of dissociation following rescattering at t_1 . Furthermore the third return peak is higher than the first return peak for either dissociation or ionization. We remark that the spectra in Fig. 10 were calculated including contributions up to four or five optical cycles after the initial tunneling ionization and convergence of the calculation was checked.

B. D^+ coincident kinetic energy spectra

The D^+ ion kinetic energy distributions in laser- D_2 interactions have been determined in coincidence measurements where the two D^+ ions were detected simultaneously by Staudte *et al.* [2] and more recently by Alnaser *et al.* [26]. In the latter experiment, the branching ratios of ionization with respect to dissociation had been measured as well, for peak laser intensities of 1-5 I_0 . Their data for peak intensity of 2.8 I_0 are shown in Figure 12. The experiment used a 35 fs pulse with mean wavelength of 800 nm. The D^+ spectra are from Coulomb explosion of ions at 60-80° with respect to the direction of the linear polarization of the laser field. In the figure we show the result of our theoretical simulation for laser intensity of 2.0 I_0 . We found best overall agreement with the experimental data at this intensity without considering volume effect and the fact that the theoretical calculation was carried out for molecules aligned perpendicular to the laser polarization while the experiments measured ions coming out of 60-80° with respect to the laser polarization. The simulated spectra near the kinetic energy peak region of 7-12 eV agree quite well with the data, but the peak near 17 eV is more pronounced in the simulation.

A direct comparison of simulated kinetic energy spectra with experimental data is complicated in general not only by the volume effect, the angular resolution of the D^+ product, but also the difficulty of knowing the peak laser intensity precisely. In Fig. 13 we show the yield

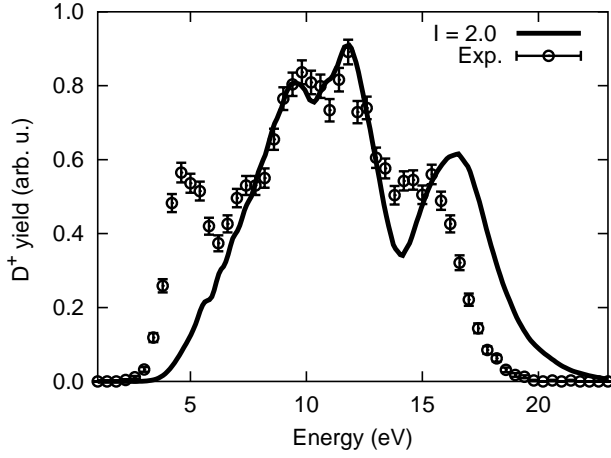


FIG. 12: Comparison of D^+ ion spectra resulting from the double ionization of D_2 molecules in a laser field. The experiment data are from Ref. [26] for peak laser intensity of $2.8 I_0$ and the theoretical simulation is for laser peak intensity of $2I_0$, where $I_0=10^{14}$ W/cm 2 and the pulse length is 35 fs.

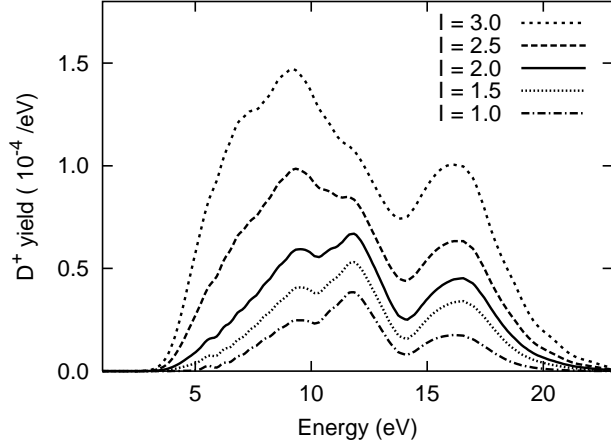


FIG. 13: Simulated D^+ ion yield from the double ionization of D_2 by the rescattering process at several peak laser intensities in units of $I_0=10^{14}$ W/cm 2 . The pulse length is 35 fs.

for making two D^+ ions vs the total kinetic energy for peak laser intensity from 1.0 - $3.0 I_0$. The calculations were done for 35 fs pulse and mean wavelength of 800 nm and with molecules aligned perpendicular to the laser polarization direction. Clearly the yield increases rapidly with laser intensity. We further note that the peak positions in the spectra do change with laser intensity. In particular, the main peak shifts to lower kinetic energy at higher laser intensity. To understand the reason of this shift, in Fig. 14 we separate the kinetic energy peaks into contributions from the σ_u and from the π_u curves, and for rescattering occurring after one, two and three optical cycles following tunneling ionization. Recall that we consider D^+ from ionization only here. At $2.0 I_0$, we note the larger contribution comes mostly from ionization of D_2^+ in the π_u state, although contribution from

σ_u is not negligible. From Fig. 14(b) one can clearly identify the two peaks approximately at 10 and 12 eV in Fig. 12 can be attributed to ionization from σ_u and π_u , respectively, for rescattering collision from the third return. At $3.0 I_0$ (Fig. 14(a)), due to the larger contribution from the σ_u excited state, the peak positions in the kinetic energy spectra are shifted to lower values. Thus the sum kinetic energy spectra at the two higher intensities look different from those at lower intensities, as seen in Fig. 13. Fig. 14(a) also shows that contribution from the third cycle becomes relatively more important at higher intensity. At higher intensity, the rescattered electron has larger kinetic energy. Thus it takes more time for the Coulomb attraction to bring the electron to come near the ion for the rescattering to occur.

Figure 14 also illustrates how the working condition for using rescattering model to measure the precise time in a molecular clock can be limited. The kinetic energy spectra from each excited electronic state of D_2^+ has relatively well specified and distinct peak positions from the first, 3rd and 5th returns. Such peak positions immediately give information about the molecular clock since each peak position does not depend on the laser inten-

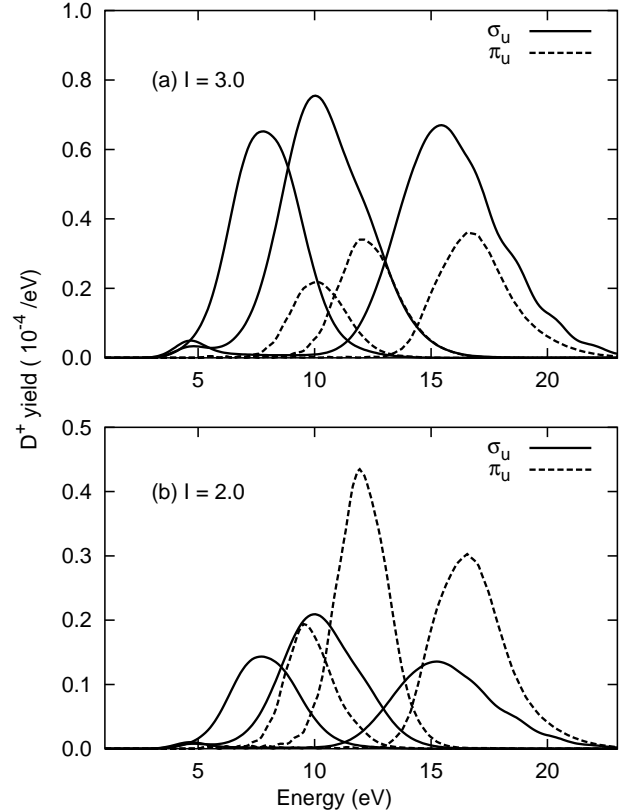


FIG. 14: D^+ yield from laser ionization via the σ_u (solid line) and π_u (dashed line) excited states with laser intensity (a) $I = 3.0 I_0$ and (b) $I = 2.0 I_0$ ($I_0=10^{14}$ W/cm 2). Each yield is further decomposed into contributions for rescattering occurring after one, two and three optical cycles. The laser pulse length is 35 fs.

sity. However, when ionization from σ_u channel also contributes then the combined sum would shift the peak positions as the laser intensity is changed, as shown in Fig. 13. Thus to read the molecular clock accurately, one has to choose laser intensity where only one of the excited D_2^+ electronic state contributes mostly to the ionization signal. Failure to do so would compromise the accuracy of the clock. Since the relative contributions of the ionization signals from σ_u and π_u are expected to change with laser intensity and with the alignment of the molecules, this also helps explain why the valleys in the experimental spectra are usually less sharply peaked than the ones simulated from the theory at a given peak laser intensity.

C. Laser- H_2 interactions and wavelength dependence

Clearly the present method can be used to predict the kinetic energy spectra if H_2 is used as the target. The only difference in H_2 is that it has smaller reduced mass such that the wave packet propagates faster, and thus kinetic energy spectra will be shifted to lower energies. If the wavelength of the laser is increased, the period is longer and thus the kinetic energy spectra also will shift to lower energies. We have applied the present theoretical model to study the comparison of kinetic energy spectra taken for H_2 and D_2 simultaneously [26], and also the variation of the kinetic energy spectra when wavelength was varied as in the experiment of Niikura *et al.* [4], see Tong *et al.* [36].

IV. SUMMARY AND CONCLUSION

In this paper we have provided a comprehensive study of the elementary processes of the rescattering mechanism leading to the fragmentation of D_2^+ following the initial tunneling ionization of a D_2 molecule in a short intense laser pulse. Ionization rates of D_2^+ from the ex-

cited electronic states and impact excitation and ionization cross sections by the returning electron have been obtained based on the MO-ADK theory and from semi-empirical formulation, respectively. Following the initial idea of Corkum and coworkers, we showed that the kinetic energy spectra of D^+ in the higher energy region (5 to 10 eV per D^+ ion) can be used as a molecular clock which can be read with subfemtosecond accuracy. Through our detailed simulation, we concluded that the dominant peak in the D^+ kinetic energy spectrum is due to the further ionization of the excited D_2^+ following impact excitation by the returning electron, and this excitation occurs not at the first return but mostly at the third return. We have compared our simulation results with the recent experiments of Niikura *et al.* and of Alnaser *et al.* with general good agreement. Further experimental studies in terms of dependence on laser wavelength, pulse duration and alignment angles may provide more critical test on the present theoretical model. From the theoretical viewpoint, despite of the semi-empirical nature of the present modeling, we do not expect any meaningful pure *ab initio* quantum calculations viable in the foreseeable future. The present model has the further advantage that the mechanism for producing each individual peaks in the kinetic energy spectra can be identified and the effect of laser parameters can be readily tested. On the other hand, the semi-empirical nature of the modeling can claim its reliability only after it has been exposed to more stringent tests from the experiment.

Acknowledgments

This work is in part supported by Chemical Sciences, Geosciences and Biosciences Division, Office of Basic Energy Sciences, Office of Science, U. S. Department of Energy. CDL also wishes to thank Igor Bray for communicating to him the partial $1s \rightarrow 2p_m$ ($m=0,1$) cross sections.

-
- [1] K. Sandig, H. Figger, and T. W. Hansch, Phys. Rev. Lett. **85**, 4876 (2000).
 - [2] A. Staudte *et al.*, Phys. Rev. A **65**, 020703(R) (2002).
 - [3] H. Niikura *et al.*, Nature **417**, 917 (2002).
 - [4] H. Niikura *et al.*, Nature **421**, 826 (2003).
 - [5] H. Sakai *et al.*, Phys. Rev. A **67**, 063404 (2003).
 - [6] J. H. Posthumus *et al.*, J. Phys. B **32**, L93 (1999).
 - [7] K. Codling, L. J. Frasinski, and P. A. Hatherly, J. Phys. B **22**, L321 (1989).
 - [8] T. Seideman, M. Y. Ivanov, and P. B. Corkum, Phys. Rev. Lett. **75**, 2819 (1995).
 - [9] T. Zuo and A. D. Bandrauk, **52**, R2511 (1995).
 - [10] E. Constant, H. Stapelfeldt, and P. B. Corkum, Phys. Rev. Lett. **76**, 4140 (1996).
 - [11] A. Giusti-Suzor *et al.*, J. Phys. B **22**, 309 (1995).
 - [12] K. Codling and L. J. Frasinski, J. Phys. B **26**, 783 (1993).
 - [13] A. Bandrauk, Comments At. Mol. Phys. **1(3)** **D**, 97 (1999).
 - [14] D. Fittinghoff, P. Bolton, B. Chang, and K. Kulander, Phys. Rev. Lett. **69**, 2642 (1992).
 - [15] K. Kondo *et al.*, Phys. Rev. A **48**, R2531 (1993).
 - [16] P. B. Corkum, Phys. Rev. Lett. **71**, 1994 (1993).
 - [17] B. Walker *et al.*, Phys. Rev. Lett. **73**, 1227 (1994).
 - [18] T. Brabec, M. Y. Ivanov, and P. B. Corkum, Phys. Rev. A **54**, R2551 (1996).
 - [19] B. Sheehy *et al.*, Phys. Rev. A **58**, 3942 (1998).
 - [20] A. Becker and F. H. M. Faisal, Phys. Rev. Lett. **84**, 3546 (2000).

- [21] R. Kopold, D. B. Milosevic, and W. Becker, Phys. Rev. Lett **84**, 3831 (2000).
- [22] G. L. Yudin and M. Y. Ivanov, Phys. Rev. A **63**, 033404 (2001).
- [23] G. L. Yudin and M. Y. Ivanov, Phys. Rev. A **64**, 035401 (2001).
- [24] L.-B. Fu, J. Liu, J. Chen, and S.-G. Chen, Phys. Rev. A **63**, 043416 (2001).
- [25] X. M. Tong, Z. X. Zhao, and C. D. Lin, Phys. Rev. A **66**, 033402 (2002).
- [26] A. Alnaser *et al.*, Phys. Rev. Lett. (2003), (in press).
- [27] A. M. Perelomov, V. S. Popov, and M. V. Terentev, Zh. Eksp. Teor. Fiz. **50**, 1393 (1966), [Sov. Phys. JETP **23**, 924 (1966)].
- [28] M. V. Ammosov, N. B. Delone, and V. P. Krainov, Zh. Eksp. Teor. Fiz. **91**, 2008 (1986), [Sov. Phys. JETP **64**, 1191 (1986)].
- [29] A. Saenz, Phys. Rev. A **61**, 051402(R) (2000).
- [30] X. Chu and S. I. Chu, Phys. Rev. A **63**, 013414 (2001).
- [31] I. Bray, CCC-database, <http://atom.murdoch.edu.au/CCC-WWW/index.html>.
- [32] Y. K. Kim, K. K. Irikura, and M. A. Ali, J. Res. NIST **105**, 285 (2000).
- [33] I. Bray, (2003), private communication.
- [34] H. Merabet *et al.*, Phys. Rev. A **60**, 1187 (1999).
- [35] J. M. Peek, Phys. Rev. **134**, A877 (1964).
- [36] X. M. Tong, Z. X. Zhao, and C. D. Lin, Phys. Rev. Lett. (2003), (in press).